VTT Technical Research Centre of Finland

Microscopic cross section calculation methodology in the Serpent 2 Monte Carlo code

Rintala, Antti; Valtavirta, Ville; Leppänen, Jaakko

Link to publication

Microscopic cross section calculation methodology in the Serpent 2 Monte Carlo code

Antti Rintala *, Ville Valtavirta, Jaakko Leppänen

VTT Technical Research Centre of Finland Ltd, P.O. Box 1000, FI-02044 VTT, Finland

ABSTRACT

This paper describes the methodology used by the Monte Carlo particle transport code Serpent to produce homogenized microscopic cross sections. The microscopic cross sections can be used for multiple purposes for example in nodal programs. The current implementation is presented together with its features and limitations. The methodology is demonstrated by calculating the activation of structural materials in two simple test problems with Serpent and the nodal neutronics program Ants utilizing Serpent-generated group constants.

© 2021 The Author(s). Published by Elsevier Ltd. This is an open access article under the CC BY-NC-ND license (http://creativecommons.org/licenses/by-nc-nd/4.0/).

1. Introduction

Production of homogenized group constants for reactor simulator calculations was the original development focus for the continuous-energy Monte Carlo particle transport code Serpent (Leppänen et al., 2015), developed at VTT Technical Research Centre of Finland Ltd (VTT). The code has been widely utilized for this application. The usual homogenized group constants calculated by Serpent include macroscopic cross sections, scattering matrices, assembly discontinuity factors and microscopic cross sections for nuclides included in certain fission product poison chains. The group constants can be calculated with both infinite lattice and leakage-corrected critical neutron spectra. (Leppänen et al., 2016).

In addition to the macroscopic cross sections, Serpent has already had the capability to calculate homogenized microscopic cross sections for user defined nuclides and reactions. Such few-group microscopic cross sections are essential in modern nodal programs for accurate modeling of reactor neutronics. Example use cases include spectral history tracking by tracking ^{239}Pu or total fissile nuclide density (Bilodid and Mittag, 2010; Bilodid et al., 2016), explicit modeling of decay heat (Bilodid et al., 2018), explicit modeling of shutdown cooling reactivity effects (Bahadir, 2015), and correction of group constants caused by the difference of tracked nuclide densities between the nodal program and single-assembly lattice calculation (Bahadir et al., 2005; Bilodid et al., 2016). All mentioned features require microscopic

depletion, i.e. tracking of the homogenized node-wise nuclide concentrations during the fuel cycle simulations with the nodal program.

Recently, the microscopic cross section homogenization with Serpent was examined in the context of utilizing the microscopic cross sections in a VTT-developed nodal neutronics program Ants (Sahlberg and Rintala, 2018). A shortcoming was discovered in the Serpent methodology, with the same finding also present in the homogenized microscopic poison cross sections produced by Serpent.

This study presents the current, revised form of the Serpent microscopic group constant homogenization routine. The usage of the cross sections in a nodal program is demonstrated in a straightforward application by modeling the activation of fuel assembly structural materials with a microscopic depletion approach. Such predictions would be difficult to make with a nodal program without the utilization of microscopic cross sections. Within two simple two-dimensional geometries, the average nuclide concentrations of structural materials are tracked fuel assembly wise using the nodal program Ants with different fixed depletion conditions. The results are compared with Serpent calculation results. The objective of this work is to present the Serpent calculation features and to demonstrate the usage of the homogenized microscopic cross sections in a nodal program, and not to estimate the achievable performance of a nodal program utilizing these cross sections.

This work is a first step towards producing estimates of nuclide-wise inventories for fuel and structural materials with a nodal program. With the flexibility of the Serpent geometry and interaction

physics descriptions, no limitations on the applicable reactor or fuel types are present. The data produced by Serpent can be post-processed to be used in any suitable nodal program.

2. Spatial homogenization of microscopic cross sections

The general idea of spatial homogenization is to preserve the reaction rates between the heterogeneous calculation with a transport program and the homogeneous calculation with for example a nodal program. A homogenized macroscopic cross section $\Sigma_{x,g}$ for reaction x and energy group g can be written as

$$\Sigma_{x,g} = \frac{\int_{E_g}^{E_{g-1}} \int_V \Sigma_x(\vec{r}, E)\phi(\vec{r}, E)\mathrm{d}V\mathrm{d}E}{\int_{E_g}^{E_{g-1}} \int_V \phi(\vec{r}, E)\mathrm{d}V\mathrm{d}E} \tag{1}$$

for a volume V to be homogenized (typically a two-dimensional fuel assembly). Here E_g and E_{g-1} are the lower and upper energy boundaries of energy group g, respectively, $\vec{r}$ represents the three- dimensional spatial coordinates, E is energy, $\Sigma_x(\vec{r}, E)$ is the macroscopic cross section for reaction x at spatial location $\vec{r}$ and neutron energy E, and $\phi(\vec{r}, E)$ is the scalar neutron flux at spatial location $\vec{r}$ and neutron energy E.

Similarly, when a microscopic cross section for a nuclide i is desired to be homogenized, the goal is to preserve the reaction rate between the heterogeneous and homogeneous representation of the same volume. When homogenizing the macroscopic cross sections the reaction rates are calculated over the whole volume V for all nuclides. The situation is slightly different for the microscopic cross sections, as they are typically desired to be homogenized only for a volume $w \in V$, where e.g. w is the fuel material and V is the fuel assembly. The homogeneous calculation has only information of V, and not of w. Therefore, the homogenized microscopic cross sections $\sigma_{x,g}^i$ have to be defined such, that the reaction rate balance

$$\sigma_{x,g}^i \overline{N^i}\,\overline{\phi}_g = \frac{1}{V}\int_{E_g}^{E_{g-1}} \int_w \sigma_x^i(\vec{r}, E)N^i(\vec{r})\phi(\vec{r}, E)\mathrm{d}V\mathrm{d}E \tag{2}$$

holds. Here $N^i(\vec{r})$ is the number density of nuclide i at $\vec{r}$, and the number density of nuclide i smeared to the homogenized volume is

$$\overline{N^i} = \frac{1}{V}\int_w N^i(\vec{r})\mathrm{d}V, \tag{3}$$

and the average neutron flux of energy group g in the homogenized volume is

$$\overline{\phi}_g = \frac{1}{V}\int_V \phi(\vec{r}, E)\mathrm{d}V. \tag{4}$$

With Eqs. (2)–(4) the homogenized microscopic cross section can be calculated as

$$\sigma_{x,g}^i = \frac{1}{\overline{N^i}\,\overline{\phi}_g}\frac{1}{V}\int_{E_g}^{E_{g-1}} \int_w \sigma_x^i(\vec{r}, E)N^i(\vec{r})\phi(\vec{r}, E)\mathrm{d}V\mathrm{d}E. \tag{5}$$

In case $N^i(\vec{r}) = 0$ in all w, the microscopic cross section is homogenized for nuclide i assuming it is evenly distributed in w. The resulting equation is

$$\sigma_{x,g}^i = \frac{1}{\overline{\phi}_g}\frac{1}{w}\int_{E_g}^{E_{g-1}} \int_w \sigma_x^i(\vec{r}, E)\phi(\vec{r}, E)\mathrm{d}V\mathrm{d}E. \tag{6}$$

This can happen for example when homogenizing transmutation cross sections for nuclides not present in fresh, zero burnup fuel. In Serpent versions earlier than 2.1.32, Eq. (6) was erroneously used also when $N^i(\vec{r}) \neq 0$ in all w. This was also the case for the homogenized microscopic fission product poison cross sections, as shown in Eq. (7) in Leppänen et al. (2016). In this case, the product of Eqs.

(3) and (6) will not generally be equal to a homogenized macroscopic cross section calculated with Eq. (1) for nuclide i only.

The integrals of Eqs. (4)–(6) are evaluated using implicit estimators. At each simulated collision, the contributions to all $\sigma_{x,g}^i$ of the collision location material are scored regardless of the reaction sampled for the neutron tracking. Therefore, the actual microscopic cross section values and nuclide densities only act as multipliers for the estimator, and their values do not affect the statistical accuracy of the resulting estimates of the homogenized microscopic cross sections.

To give a simple demonstration of the effect of erroneously applying Eq. (6) instead of Eq. (5), an EPR type single fuel assembly input from Serpent Wiki (2021) is utilized. A fixed condition burnup calculation is performed with equilibrium ^{135}Xe density for the fuel assembly containing 20 fuel rods with Gd burnable poison (PB). A burnup calculation is performed for an otherwise similar model, but with the PB rods replaced with regular UO_2 rods. The homogenized thermal microscopic absorption cross section of ^{135}Xe ($\sigma_{a,2}^{Xe}$) is calculated with the old implementation (Eq. (6)) and the new implementation (Eq. (5)). The resulting homogenized microscopic cross sections are shown in Fig. 1 for both cases and both implementations, together with the differences between the implementations.

The discrepancy of applying the different equations is much smaller for the uniformly enriched fuel assembly, as the only cause for the heterogeneous distribution of the ^{135}Xe density is the control rod guide tubes in the fuel lattice. However, the difference slightly grows with increasing burnup. For the more heterogeneous case with PB rods, the difference is much more pronounced. The difference is at its greatest at the beginning of the burnup calculation, and is lessened with the depletion of Gd. The $\sigma_{a,2}^{Xe}$ values of the PB and no PB cases approach each other towards the end of the calculation, where the differences between the new and the old methods are practically equivalent for both PB and no PB cases.
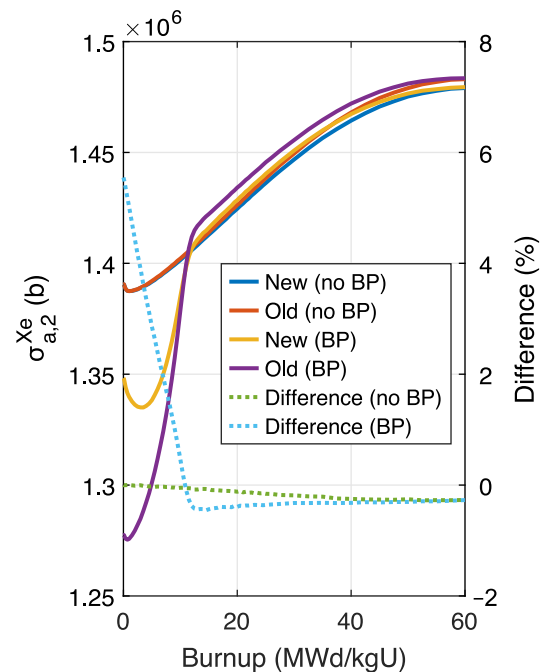

Fig. 1. Homogenized thermal microscopic absorption cross section of ^{135}Xe ($\sigma_{a,2}^{Xe}$) for a fuel assembly without PB rods and with PB rods calculated using Eq. (5) (New) and Eq. (6) (Old). The relative differences (New/Old $-$ 1) $\times$ 100% are plotted on the right y axis.

3. Features and limitations

Serpent calculates the homogenized microscopic cross sections for user-specified nuclides and reactions, identified with ENDF format reaction types specified with MT numbers. Additionally, the smeared nuclide densities of Eq. (3) are calculated. Separate cross sections can be calculated for reactions where the resulting nuclide is in ground or isomeric state. The homogenized microscopic fission cross sections can be calculated for total fission cross section, or separately for fission reactions resulting in the use of the different energy-dependent fission product yield data by Serpent. The available energy-dependent fission product yields are determined by the ENDF format neutron-induced fission yield library file for the nuclide. The fission yields and radioactive decay data are also included in the Serpent output to ease the post-processing of data for a nodal program. Additional special reactions are the fission neutron production cross section $v\sigma_{\mathrm{f},g}^i$ for total, delayed or prompt v, and fission energy production cross section $\kappa\sigma_{\mathrm{f},g}^i$.

The most obvious limitation in the current implementation is that only microscopic reaction cross sections can be calculated. The implementation lacks the support for nuclide-wise scattering matrices and diffusion coefficients. As opposed to the macroscopic group constants, the microscopic cross sections are homogenized directly in the desired few-group structure with the actual neutron flux spectrum present in the calculation. The macroscopic group constants are first tallied into a multi-group structure, which can be condensed into a few-group spectrum either with the infinite lattice neutron flux spectrum or a leakage-corrected critical spectrum. Therefore, the leakage-corrected critical neutron spectrum can not be used to collapse the homogenized microscopic cross sections.

Furthermore, the usage of the microscopic cross section calculation feature is somewhat more complicated than the calculation of the macroscopic group constants. An example case could be the modeling of all possible reactions of a system. The full input will depend on the nuclide composition of the problem and on cross section library data in use, as the available reaction cross sections depend on these settings. In contrast, the macroscopic group constants are always similarly calculated independent of the nuclide content of the problem and the used cross section library.

The user should also be aware of the properties of the collision flux estimator used in Serpent especially when calculating microscopic cross sections in optically thin materials without neutron sources and for reactions with high threshold energy. The resulting cross sections might have very high statistical uncertainties, or be altogether erroneously zero due to lack of scores at these materials with high neutron energies. One possibility to overcome this complication is to reduce the minimum mean distance for scoring the collision flux estimator (Leppänen, 2017). This will however result into a higher computational expense of the homogenization calculation in usual reactor applications.

4. Demonstration

The methodology is demonstrated by comparing Serpent simulation results to those calculated with the nodal neutronics program Ants. Two-group homogenized macroscopic constants and microscopic cross sections calculated with Serpent are used in Ants. Two simple infinite two-dimensional geometries consisting of pressurized water reactor fuel assemblies from the BEAVRS benchmark (Horelik et al., 2013) are used as test cases. The goal is to model the activation of structural materials.
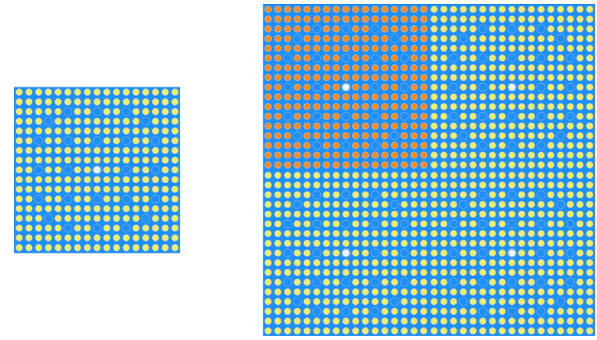
Fig. 2. Serpent geometry plots of the first (left) and second (right) test problems. Both problems have reflective boundary conditions. The yellow and orange pins have 2.4 % and 3.4 % ^{235}U enrichments, respectively.

4.1. Problem geometries

The first geometry is a single 2.4 % ^{235}U enriched assembly with reflective boundary conditions. The second geometry has one 3.4 % ^{235}U enriched assembly and three 2.4 % ^{235}U enriched assemblies surrounded by reflective boundary conditions. In contrast to the benchmark specifications, the Zircaloy structural material compositions were defined accurately taking impurities also into account. Serpent geometry plots of the problems are shown in Fig. 2. Power density of both problems is 41.7 W/kgU.

4.2. Group constants

The Ants models use a simplified group constant model with similar parametrization as used in the legacy nodal simulator program HEXBU-3D/MOD5 (Kaloinen, 1992). Both the macroscopic and microscopic data are presented with independent second order polynomial fits for fuel temperature, boron density, and coolant density combined with the effect of coolant temperature.
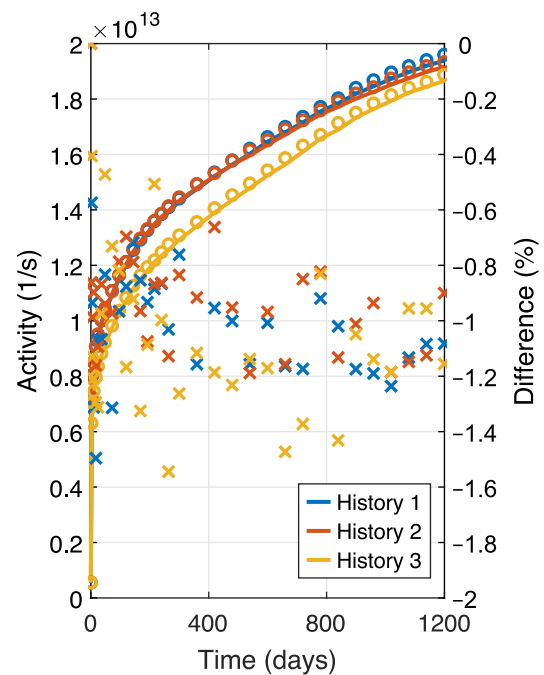
Fig. 3. Total structural material activities for the different history calculations of the first test problem. Solid lines: Ants results, circles: Serpent results, crosses: relative differences Ants–Serpent (right axis).
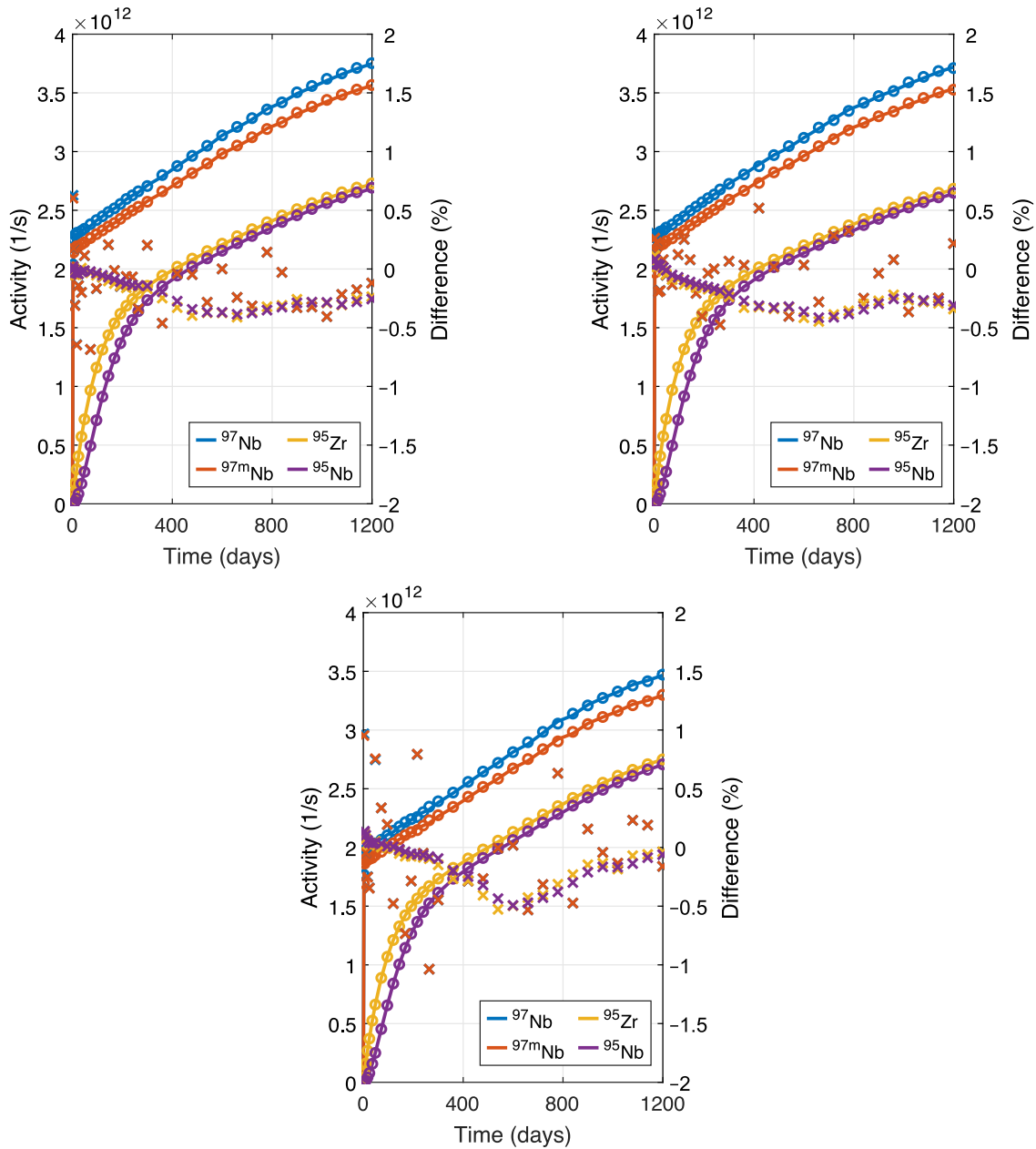
Fig. 4. Selected nuclide activities during the different history calculations for the first test problem. Top left: history 1, top right: history 2, bottom: history 3. Solid lines: Ants results, circles: Serpent results, crosses: relative differences Ants–Serpent (right axis).

One cross term is present for boron and coolant densities. A simplified ^{239}Pu history model similar to the one described in Bilodid and Mittag (2010) is used. The polynomials are fitted at each considered burnup to the results of 8 different state point calculations, including the nominal depletion state point. The state points are of the form lower and higher fuel temperature, lower and higher boron density, and lower coolant density with higher coolant temperature and higher coolant density with lower cool-

ant temperature. One cross variation of boron and coolant density is included for the cross term evaluation. The nominal data and the polynomial coefficients are tabulated with respect to burnup, and the values between the tabulated burnups are linearly interpolated in Ants. The nominal data use a denser burnup grid than the polynomial coefficients. The group constant calculations were performed with 10^6 neutrons per cycle and with 100 active and 25 inactive cycles.

Table 1
Maximum values of total and selected nuclide activity differences |Ants/Serpent − 1| × 100 % during the different history calculations for the first test problem.

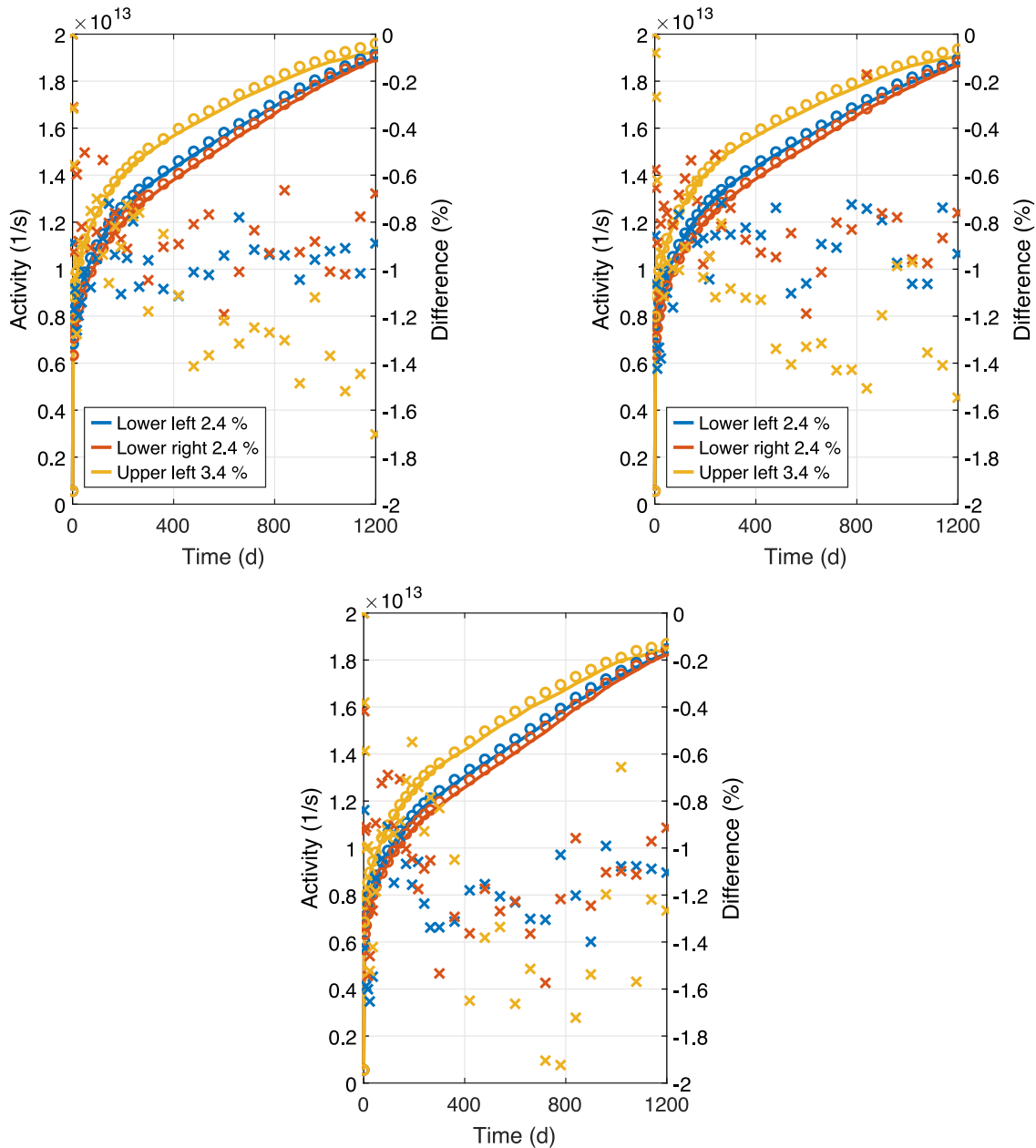| History	Total	^{97}Nb	^{97m}Nb	^{95}Zr	^{95}Nb
1	1.50	0.69	0.68	0.41	0.39
2	1.19	0.52	0.52	0.45	0.41
3	1.54	1.04	1.04	0.53	0.49

Fig. 5. Total structural material activities of the fuel assemblies for the different history calculations of the second test problem. Top left: history 1, top right: history 2, bottom: history 3. Solid lines: Ants results, circles: Serpent results, crosses: relative differences Ants–Serpent (right axis).

For the ^{239}Pu history model, the homogenized microscopic $(n, 2n), (n, \gamma)$ and (n, f) cross sections of nuclides ^{239}U, ^{239}Np and ^{239}Pu are calculated for the fuel materials. For modeling the structural material activation, all possible reactions for the nuclides in the structural materials are included in the microscopic cross section calculation. JEFF-3.2 cross section data files were used with JEFF-3.1.1 fission product yield and radioactive decay data files. The total number of nuclides with non-zero cross sections was 469 with 7208 reactions. Including all possible decay paths, a total of 1154 nuclides are included in the Ants microscopic depletion calculations. No nuclides with fission reactions were present. For both the ^{239}Pu history and the structural material activation model the zero burnup smeared nuclide densities are used from the Serpent data to initialize the nuclide number densities in the Ants models. The group constants of the fuel assemblies are not corrected with the actual nuclide density differences in the structural materials.

4.3. Calculation setups

The Serpent reference depletion calculations used incomplete partial fractions (IPF) form of the Chebyshev rational approximation method (CRAM) of order 16 (Pusa, 2016). The linear extrapolation and linear interpolation depletion algorithm was used with 10 substeps in both predictor and corrector (Isotalo and Aarnio, 2011a,b). Ants used constant extrapolation depletion algorithm with order 16 IPF CRAM. 20 depletion steps per Serpent depletion step was used in Ants to diminish the effect between the different depletion algorithms. In the Serpent depletion calculations, each fuel material in each fuel pin and each Zircaloy cladding in each fuel or guide tube pin forms their own depletion zone. In Ants calculations the microscopic depletion is calculated separately for the fuel and structural material in each fuel assembly. The Serpent reference calculations were performed with 100 active and 25 inac-
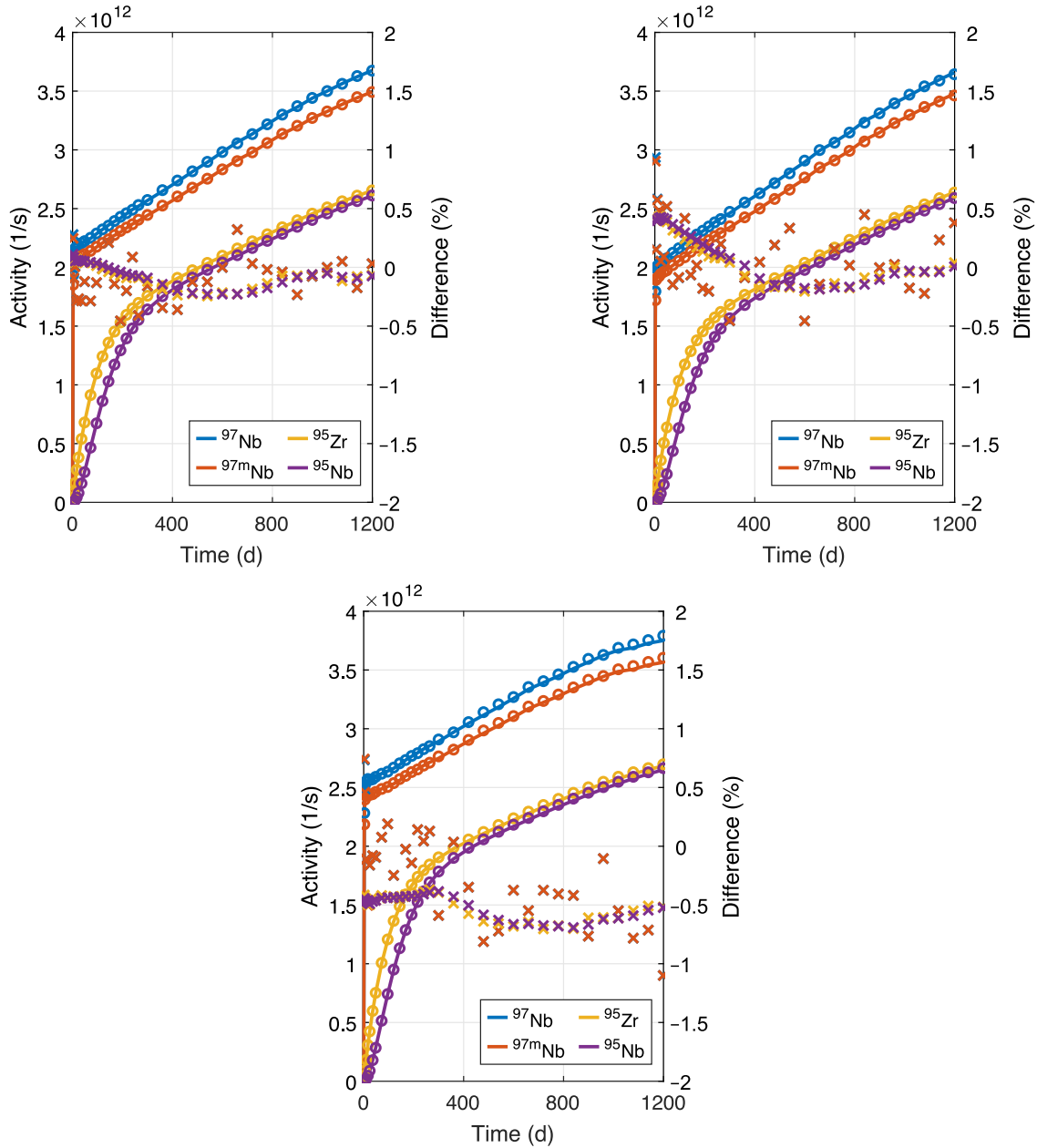
Fig. 6. Selected nuclide activities during the first history calculation of the second test problem. Top left: lower left 2.4 % fuel assembly, top right: lower right 2.4 % fuel assembly, bottom: upper left 3.4 % fuel assembly. Solid lines: Ants results, circles: Serpent results, crosses: relative differences Ants–Serpent (right axis).

tive cycles and with 10^6 and 4×10^6 neutrons per cycle of the first and second test problem, respectively.

4.4. Results

Three comparison calculations with different fixed historical thermal hydraulic conditions were performed for both geometries. The first history is the same as the nominal depletion state point during the group constant generation. The second history is otherwise similar, but the higher fuel temperature of the group constant generation is used. The third history has zero boron density and high coolant density and low coolant temperature. The state points of the two last histories are also included in the group constant generation. However, the historical depletion conditions are different than during the group constant generation. Equilibrium ^{135}Xe densities are used in all calculations.

The compared results of the test calculations are the total structural material activity of the 925 considered decaying nuclides and the activities of nuclides selected from the most active nuclides: ^{97}Nb, ^{97m}Nb, ^{95}Zr and ^{95}Nb.

For the first test problem the total activities are shown in Fig. 3 and the nuclide activities in Fig. 4. The maximum relative differences are presented in Table 1. The differences of the first two histories are rather similar. The second history has similar conditions in the structural material as in the first history, whereas the spectrum is slightly different due to the different fuel temperature. With the third history, where the conditions are different also in the structural material and coolant, the differences are more pronounced. The maximum differences of ^{95}Zr and ^{95}Nb are closer to zero and the differences are more smoothly varying in time than those of ^{97}Nb and ^{97m}Nb. Both the activities and the maximum relative differences of the two latter nuclides are greater than for the
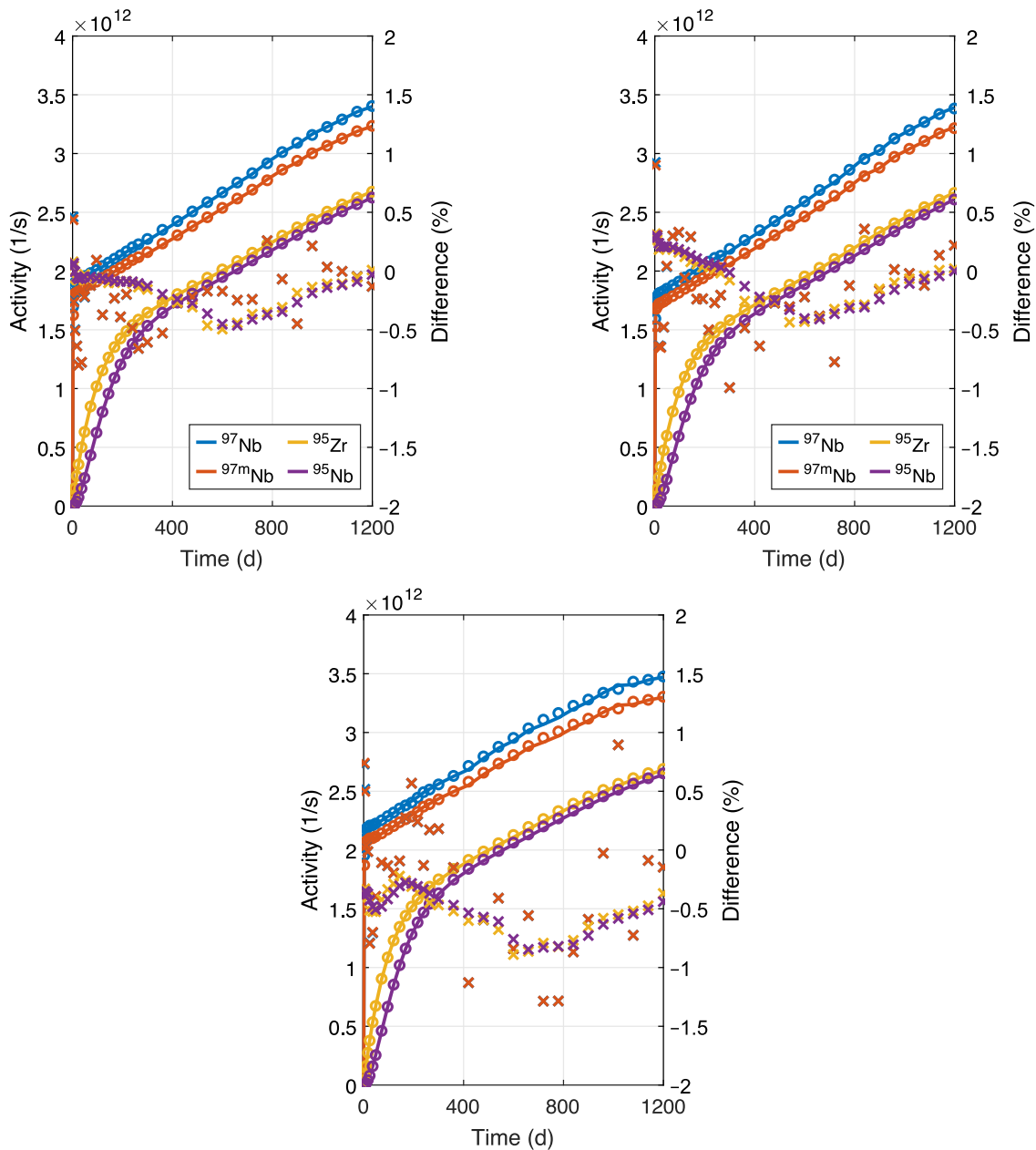
Fig. 7. Selected nuclide activities during the third history calculation of the second test problem. Top left: lower left 2.4 % fuel assembly, top right: lower right 2.4 % fuel assembly, bottom: upper left 3.4 % fuel assembly. Solid lines: Ants results, circles: Serpent results, crosses: relative differences Ants–Serpent (right axis).

two former nuclides. Especially the two first histories show rather similar behavior between Serpent and Ants. The third history with the largest deviation from the nominal group constant depletion state point show more variation in the differences of successive time steps. This is most likely caused by inadequate Monte Carlo method statistics of the homogenized microscopic cross sections

Table 2
Maximum values of total and selected nuclide activity differences |Ants/Serpent − 1| × 100 % during the different history calculations for the second test problem for the different fuel assemblies. LL: lower left fuel assembly, LR: lower right fuel assembly, UL: upper left fuel assembly.

History	Assembly	Total	^{97}Nb	^{97m}Nb	^{95}Zr	^{95}Nb
1	LL 2.4 %	1.26	0.46	0.46	0.24	0.23
	LR 2.4 %	1.42	0.94	0.90	0.43	0.43
	UL 3.4 %	1.65	1.10	1.10	0.70	0.69
2	LL 2.4 %	1.19	0.54	0.54	0.24	0.23
	LR 2.4 %	1.19	1.33	1.33	0.54	0.55
	UL 3.4 %	1.57	1.00	1.01	0.78	0.73
3	LL 2.4 %	1.70	0.80	0.80	0.49	0.46
	LR 2.4 %	1.55	0.99	0.99	0.44	0.41
	UL 3.4 %	1.92	1.29	1.29	0.89	0.85

for some nuclides for the optically thin volumes of the structural materials as mentioned in Section 3.

The presented results for the first test problem are mostly rather consistently underpredicted by Ants. Some of the differences might be caused by the statistical accuracy of the homogenized microscopic cross sections. However, three differences between Ants and Serpent depletion calculations may all partly explain the differences. First, the higher order depletion methods in Serpent are not yet implemented in Ants (Isotalo and Aarnio, 2011a,b). This effect has been compensated by performing the Ants calculations with a denser time stepping, as mentioned in Section 4.3. This leads to the second difference, where the equilibrium ^{135}Xe densities are also updated with denser time stepping than in Serpent. Finally, the linear interpolation of all group constant data with regards to burnup in Ants might lead to the misprediction of some reaction rates between the tabulated burnup values, if the microscopic cross sections are considerably and non-linearly changing between the burnup values.

The second test problem differs from the first in the sense that one of the four assemblies has a higher enrichment, thus producing leakage between the assemblies. The total structural material activities are shown in Fig. 5 and the selected nuclide activities in Figs. 6 and 7 for the first and third histories. The maximum relative differences are presented in Table 2.

The errors are generally higher for the higher enrichment assembly. Additionally the differences are greater in the second test problem than in the first. Otherwise similar observations of the results are present as with the first test problem. The nuclides ^{97}Nb and ^{97m}Nb have higher differences when compared with those of ^{95}Zr and ^{95}Nb, with some fluctuation in the Ants values. The differences are more pronounced in the third history with the largest departure of the thermal hydraulics conditions from the nominal group constant calculation. The total activities are underpredicted by Ants in all histories and assemblies. The underprediction trend was also seen in some of the nuclide-wise activities.

The general trend of the activity results was rather similar between the problems. The observations on the homogenized microscopic cross section calculations for the optically thin volumes of the structural materials and the differences in the burnup algorithms between Ants and Serpent also hold in the second test problem. Differences in the difference behaviors between the different fuel assemblies in the second test problem are explained by the application of the nodal method in Ants, compared with the heterogeneous representation in Serpent.

The results demonstrate that the homogenized microscopic cross sections generated by Serpent can be used by a nodal program to successfully predict the evolution of nuclide densities and activities of materials that are not spatially resolved in the nodal solution. The agreement between direct spatially resolved continuous-energy Monte Carlo and spatially homogenized nodal diffusion methods can be considered reasonable for this demonstration.

5. Summary and conclusions

A revised form of the homogenized microscopic cross section calculation routine in Serpent has been introduced in this work. The methodology is applied to fission product poison cross section calculations as well as to user defined nuclides and reactions. The features and limitations of the methodology were shortly introduced. The microscopic cross sections produced by Serpent can be used in nodal programs for multiple applications, including the modeling of historical effects.

As a methodology demonstration, the Serpent-generated homogenized microscopic cross sections were used in the nodal neutronics program Ants in two test problems to model the activation of structural materials. The total activities and selected nuclide activities were presented. The results are promising, however the statistical uncertainties of the applied microscopic cross sections should still be investigated. The root cause for the rather consistent underprediction trend of the Ants results should also be studied in order to improve the agreement between Ants and Serpent. The applying of the methodology for modeling the structural material activation in a real reactor geometry will still require considerable amount of verification work.

CRediT authorship contribution statement

Antti Rintala: Conceptualization, Methodology, Formal analysis, Investigation, Writing - original draft, Software, Visualization. **Ville Valtavirta:** Conceptualization, Methodology, Software, Writing - review & editing. **Jaakko Leppänen:** Methodology, Software, Writing - review & editing.

Declaration of competing interest

The authors declare that they have no known competing financial interests or personal relationships that could have appeared to influence the work reported in this paper.

Acknowledgments

References

Bahadir, T., 2015. Modeling of shutdown cooling reactivity effects with SIMULATE, in: PHYSOR 2014..

Bahadir, T., Lindahl, S., Palmtag, S.P., 2005. SIMULATE-4 multigroup nodal code with microscopic depletion model. Mathematics and Computation, Supercomputing, Reactor Physics and Nuclear and Biological Applications..

Bilodid, I., Mittag, S., 2010. Use of the local Pu-239 concentration as an indicator of burnup spectral history in DYN3D. Ann. Nucl. Energy 37, 1208–1213.

Bilodid, Y., Kotlyar, D., Shwageraus, E., Fridman, E., Kliem, S., 2016. Hybrid microscopic depletion model in nodal code DYN3D. Ann. Nucl. Energy 92, 397–406.

Bilodid, Y., Fridman, E., Kotlyar, D., Shwageraus, E., 2018. Explicit decay heat calculation in the nodal diffusion code DYN3D. Ann. Nucl. Energy 121, 374–381.

Horelik, N., Herman, B., Forget, B., Smith, K., 2013. Benchmark for evaluation and validation of reactor simulations (BEAVRS), v1.0.1, in: Int. Conf. Mathematics and Computational Methods Applied to Nuc. Sci. & Eng, pp. 5–9..

Isotalo, A.E., Aarnio, P.A., 2011a. Higher order methods for burnup calculations with Bateman solutions. Ann. Nucl. Energy 38, 1987–1995.

Isotalo, A.E., Aarnio, P.A., 2011b. Substep methods for burnup calculations with Bateman solutions. Ann. Nucl. Energy 38, 2509–2514.

Kaloinen, E., 1992. New version of the HEXBU-3D code. In: Proceedings of the second Symposium of AER, pp. 9–22.

Leppänen, J., 2017. On the use of delta-tracking and the collision flux estimator in the Serpent 2 Monte Carlo particle transport code. Ann. Nucl. Energy 105, 161–167.

Leppänen, J., Pusa, M., Viitanen, T., Valtavirta, V., Kaltiaisenaho, T., 2015. The Serpent Monte Carlo code: Status, development and applications in 2013. Ann. Nucl. Energy 82, 142–150.

Leppänen, J., Pusa, M., Fridman, E., 2016. Overview of methodology for spatial homogenization in the Serpent 2 Monte Carlo code. Ann. Nucl. Energy 96, 126–136.

Pusa, M., 2016. Higher-order Chebyshev rational approximation method and application to burnup equations. Nucl. Sci. & Eng. 182, 297–318.

Sahlberg, V., Rintala, A., 2018. Development and first results of a new rectangular nodal diffusion solver of Ants, in: PHYSOR2018, pp. 3861–3871..

Serpent Wiki, 2021. Tutorial - Serpent Wiki. (Accessed 2021-06-24)..